engineering proceedings

MDPI

Proceeding Paper

Reduced-Order Active Disturbance Rejection Control for the Roll Channel of Small Fixed-Wing UAVs †

Furkan Leblebici [1,2,‡] and Ozan Tekinalp [2,*,‡]

[1] ROKETSAN A.S., 06780 Ankara, Türkiye; furkan.leblebici@roketsan.com.tr
[2] Department of Aerospace Engineering, Middle East Technical University, 06800 Ankara, Türkiye
* Correspondence: tekinalp@metu.edu.tr
† Presented at the 15th EASN International Conference, Madrid, Spain, 14–17 October 2025.
‡ These authors contributed equally to this work.

Abstract

Roll autopilots of small fixed-wing unmanned aerial vehicles (UAVs) should reject roll disturbances and compensate for parameter variations during flight. This study investigates an active disturbance rejection control (ADRC) architecture based on an extended state observer (ESO), with emphasis on a reduced-order ESO (RESO), for the roll channel of a small fixed-wing UAV. The roll axis is represented by a first-order roll-rate model augmented with actuator and rate-gyro dynamics; a proportional–derivative law is applied to the tracking error, while an extended state observer estimates a lumped total disturbance, and this estimate is fed forward for real-time disturbance compensation. Two observer designs are considered: a second-order linear ESO (LESO) and a first-order RESO using roll-rate and actuator feedback. Frequency-domain and time-domain analyses are carried out under aerodynamic uncertainty, actuator limits, sensor noise, and sinusoidal roll disturbances, and the RESO-based ADRC is compared with LESO-ADRC, a linear quadratic integral (LQI) controller, and a classical proportional–integral–derivative (PID) design. The simulations show that the RESO implementation retains the disturbance rejection and robustness of LESO-ADRC while reducing the observer order, and it offers improved disturbance rejection capability with acceptable noise sensitivity. These properties make RESO-based ADRC a promising candidate for real-time roll autopilots in small fixed-wing UAV applications.

Keywords: active disturbance rejection control; reduced-order extended state observer; roll autopilot; fixed-wing UAV

Check for updates

Academic Editors: Spiros Pantelakis, Andreas Strohmayer and Gustavo Alonso

Published: 7 May 2026

Copyright: © 2026 by the authors. Licensee MDPI, Basel, Switzerland. This article is an open access article distributed under the terms and conditions of the Creative Commons Attribution (CC BY) license.

1. Introduction

The roll autopilot is one of the critical inner-loop controllers for air vehicles, responsible for rolling the aircraft to a commanded roll angle ϕ. In practice, airframes often exhibit weakly damped dynamics in the roll channel, which makes this axis sensitive to asymmetric aerodynamic loads, fin misalignment, and aerodynamic turbulence. Together with these external disturbances, aerodynamic uncertainties and sensor dynamics can degrade autopilot performance. Therefore, a robust roll autopilot should be able to reject such effects in the presence of sensor noise and aerodynamic uncertainty [1–3].

In both the academic literature and industrial practice, roll autopilots are most commonly implemented using proportional–integral–derivative (PID) control combined with gain scheduling. Although this structure is simple to implement, its performance typically

degrades in the presence of parametric uncertainties and external disturbances. In several reported unmanned aerial vehicle (UAV) and missile-related roll-control studies, PID-based roll autopilots have failed to maintain accurate roll tracking under significant disturbance inputs [4,5]. Han proposed active disturbance rejection control (ADRC), a model-free control architecture that provides strong disturbance rejection by actively estimating and compensating for the total disturbance acting on the system [6].

ADRC represents the combined effect of internal uncertainties and external disturbances as the total disturbance, which is estimated in real time by an extended state observer (ESO) and compensated in a feedforward manner through the control input [6,7]. ESO-based controller designs have been applied to various aerospace and marine vehicle-control problems [1,4,8–11], usually with performance evaluated in the time domain for standard disturbances such as step torques or sinusoidal excitations [1,11].

Several reported studies focus on time-domain performance and only indirectly address frequency-domain metrics such as stability margins, disturbance rejection characteristics, and noise attenuation for the aircraft autopilot [1,4,8,11,12]. These properties are largely discussed qualitatively rather than quantified for specific autopilot designs. Additionally, while reduced-order observers have been considered in other control problems, systematic comparisons between full-order ESO and reduced-order ESO structures in aircraft roll autopilots are still limited. The present study provides a detailed frequency-domain characterization of an ADRC-based roll autopilot, explicitly examines the disturbance/noise trade-off, and compares the ADRC design against both PID and linear quadratic integral (LQI) controllers on an identical plant model.

This work designs and analyzes a robust roll autopilot for a small fixed-wing UAV. The roll dynamics are represented as a first-order plant augmented with servo and sensor dynamics, while all aerodynamic variations and external torques are treated as a lumped disturbance. Two linear ADRC architectures are considered: one based on a conventional second-order ESO (LESO) and another based on a reduced-order ESO (RESO). Both structures are benchmarked against LQI and PID controllers, whose parameters are obtained via constrained nonlinear optimization. The analysis is carried out in both the frequency domain and the time domain, including the effects of aerodynamic uncertainty, gyro, and actuator dynamics. The results indicate that the RESO-based ADRC retains the robust performance of the LESO scheme and provides improved low-frequency disturbance rejection compared to LQI and PID, while keeping noise rejection capability at an acceptable level. The scope of this paper is limited to generic roll-channel flight-control and autopilot analysis for a small fixed-wing UAV model.

2. Materials and Methods

2.1. Roll-Channel Dynamic Model

The lateral dynamics of the fixed-wing UAV are modeled under the assumptions of small angles, decoupled roll, pitch, and yaw channels, and negligible sideslip. The linearized roll-rate dynamics around a trim condition are given by [13]

$$\dot{p} = L_p\, p + L_\delta\, \delta \tag{1}$$

where p is the roll rate, δ is the aileron deflection, $L_p < 0$ is the roll-damping derivative, and L_δ is the control-effectiveness derivative. The dimensional rolling moment about the body x-axis is written as $L = q_\infty S b\, C_\ell$, with dynamic pressure $q_\infty = \frac{1}{2}\rho V^2$, reference area S, wing span b, and roll-moment coefficient $C_\ell \approx C_{\ell_p}\, \frac{pb}{2V} + C_{\ell_\delta}\, \delta$. Using the roll moment of inertia I_{xx} and $I_{xx}\dot{p} = L$, the linear roll dynamics in (1) can be expressed in the form $L_p = \frac{q_\infty S b^2}{2 I_{xx} V}\, C_{\ell_p}, L_\delta = \frac{q_\infty S b}{I_{xx}}\, C_{\ell_\delta}$.

https://doi.org/10.3390/engproc2026133085

Taking the Laplace transform of (1), the transfer functions from aileron deflection to roll rate and roll angle become

$$\frac{p(s)}{\delta(s)} = \frac{L_\delta}{s - L_p}, \qquad \frac{\phi(s)}{\delta(s)} = \frac{L_\delta}{s\,(s - L_p)}. \tag{2}$$

The servo actuator is modeled as a second-order system: $\frac{\delta(s)}{\delta_c(s)} = \frac{\omega_{\text{cas}}^2}{s^2+2\zeta_{\text{cas}}\omega_{\text{cas}}s+\omega_{\text{cas}}^2}$, where δ_c is the commanded aileron deflection, and ω_{cas} and ζ_{cas} are the actuator natural frequency and damping ratio, respectively. The rate-gyro dynamics are similarly modeled as a second-order transfer function with natural frequency ω_{gyro} and damping ratio ζ_{gyro}, which introduce sensor lag and additional phase loss.

2.2. Linear Extended State Observer and Total Disturbance

The roll dynamics with uncertain aerodynamic parameters can be expressed as

$$\begin{cases} \dot{p} = -a_0\, p - a_1\, \phi + b\, u, \\ \dot{\phi} = p, \\ y_1 = p, \end{cases} \tag{3}$$

where $[\,p \;\; \phi\,]^\top$ is the state vector, y_1 is the measured roll rate, u is the control input (aileron control moment obtained from actuator encoder feedback), b is the control-effectiveness gain (nominally related to L_δ), and a_0 and a_1 are uncertain aerodynamic parameters.

Following the ADRC principle [6], the term $f(p, \phi) = -a_0 p - a_1 \phi$ is treated as the *total disturbance*, which includes modeling errors, aerodynamic parameter variations, unmodeled couplings, and external roll disturbances. The objective of the LESO is to estimate f in real time and compensate for it in the control law.

2.3. Second-Order Linear Extended State Observer

When both roll rate p and roll angle ϕ are available for feedback, a second-order linear ESO can be constructed based on the roll-rate measurement p. Let z_1 denote an estimate of p and z_2 an estimate of the total disturbance f. The second-order LESO is given by

$$\begin{cases} \dot{z}_1 = z_2 - \beta_1\,(z_1 - p) + b\, u, \\ \dot{z}_2 = -\,\beta_2\,(z_1 - p), \end{cases} \tag{4}$$

where β_1 and β_2 are observer gains selected to achieve a desired observer bandwidth, and u is the control input measured from the actuator.

2.4. Reduced-Order Extended State Observer (RESO)

Similarly, when both roll rate p and roll angle ϕ are available for feedback, since the main idea is to estimate the total disturbance $f(p, \phi)$, a first-order extended state observer can be designed for estimating $f(p, \phi)$ by $\tilde{z}_2$.

The first-order ESO (RESO) is defined as

$$\left.\begin{cases} \dot{\tilde{z}}_1 = -\,\beta_{\text{RESO}}\,\tilde{z}_1 - \beta_{\text{RESO}}^2\, p - \beta_{\text{RESO}}\, b\, u \\ \tilde{z}_2 = \tilde{z}_1 + \beta_{\text{RESO}}\, p, \end{cases}\right\} \tag{5}$$

where $\beta_{\text{RESO}} > 0$ is the RESO bandwidth parameter. Compared with the LESO in (4), the RESO has one fewer dynamic state, which simplifies implementation and can improve robustness by increasing the phase margin [14].

https://doi.org/10.3390/engproc2026133085

2.5. Active Disturbance Rejection Control

The roll-attitude controller is chosen as a PD law acting on the roll-angle tracking error: $e_\phi = \phi_{\text{com}} - \phi$. The ADRC control law augments this feedback with disturbance compensation using the ESO/RESO estimate. Denoting the disturbance estimate by $\hat{f}$ ($\hat{f} = z_2$ for the LESO; $\hat{f} = \tilde{z}_2$ for the RESO), the control input is

$$u_{\text{ADRC}} = \frac{K_p\,(\phi_{\text{com}} - \phi) - K_d\,p - \hat{f}}{b_0}, \tag{6}$$

where K_p and K_d are proportional and derivative gains, respectively, and b_0 is the nominal control-effectiveness gain.

The resulting closed-loop structure consists of the roll-channel plant, actuator and gyro dynamics, the linear extended state observer, and the PD-based ADRC law, as shown schematically in Figure 1. The signal d_{external} represents external roll-disturbance inputs acting on the airframe, while $n_{\dot{\phi}}$ denotes the gyro rate measurement noise.

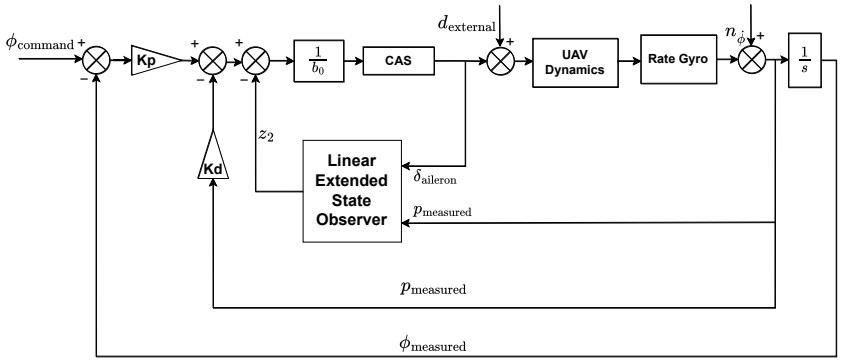


Figure 1. Block diagram of the active disturbance rejection controller (ADRC) for the roll channel, including the plant, actuator, and gyro dynamics, and linear extended state observer.

2.6. Benchmark Controllers: LQI and PID

To compare the RESO–ADRC performance, an LQI controller and a classical PID controller are designed using the same roll-channel model. The LQI control law is $u(t) = K_I \int_0^t \left(\phi_{\text{com}}(\tau) - \phi(\tau)\right) d\tau \;-\; K_1\,\phi(t) \;-\; K_2\,p(t) \;-\; K_3\,\delta(t) \;-\; K_4\,\dot{\delta}(t)$ where K_I is the integral gain and $K_1, \ldots, K_4$ are feedback gains obtained from a linear quadratic design with integral action that accounts for actuator states. In addition, the PID controller is implemented as $u(t) = K_P\,e(t) + K_I \int_0^t e(\tau)\,d\tau + K_D\,\frac{de(t)}{dt}$, where $e(t) = \phi_{\text{com}}(t) - \phi(t)$ is the roll-angle error and K_P, K_I, and K_D are tuned to satisfy time-domain and frequency-domain specifications. All controllers are designed to satisfy common design criteria summarized in Table 1, including phase and gain margins, actuator constraints, and overshoot limits.

Table 1. Design criteria for controller tuning.

Parameter	Design Criterion
Phase margin	$\geq 60^\circ$
Gain-margin magnitude	≥ 6 dB
Maximum actuator rate and deflection	$\dot{\delta}_{\max} \leq 40^\circ/\text{s}$, $\delta_{\max} = \pm 10^\circ$
Overshoot	$\leq 10\%$

Controller tuning is performed in MATLAB [15] using the `fmincon` routine (Find minimum of constrained nonlinear multivariable function). The design constraints listed in Table 1 are implemented as bound and inequality constraints, and an optimization problem is formulated with the objective of maximizing the closed-loop bandwidth of the roll-rate

loop. To reduce the risk of convergence to poor local optima, the optimization is started from several different initial points for each controller structure, and the best feasible solution is found. For the ADRC-based designs, additional constraints are added on the extended state observer (ESO). In line with common ADRC design guidelines, which recommend choosing the observer bandwidth approximately five to ten times higher than the controller bandwidth in order to balance disturbance estimation speed and noise sensitivity [16], the ESO bandwidth value is selected to be about 5 times that of the closed system.

3. Results and Discussion

3.1. Model Parameters

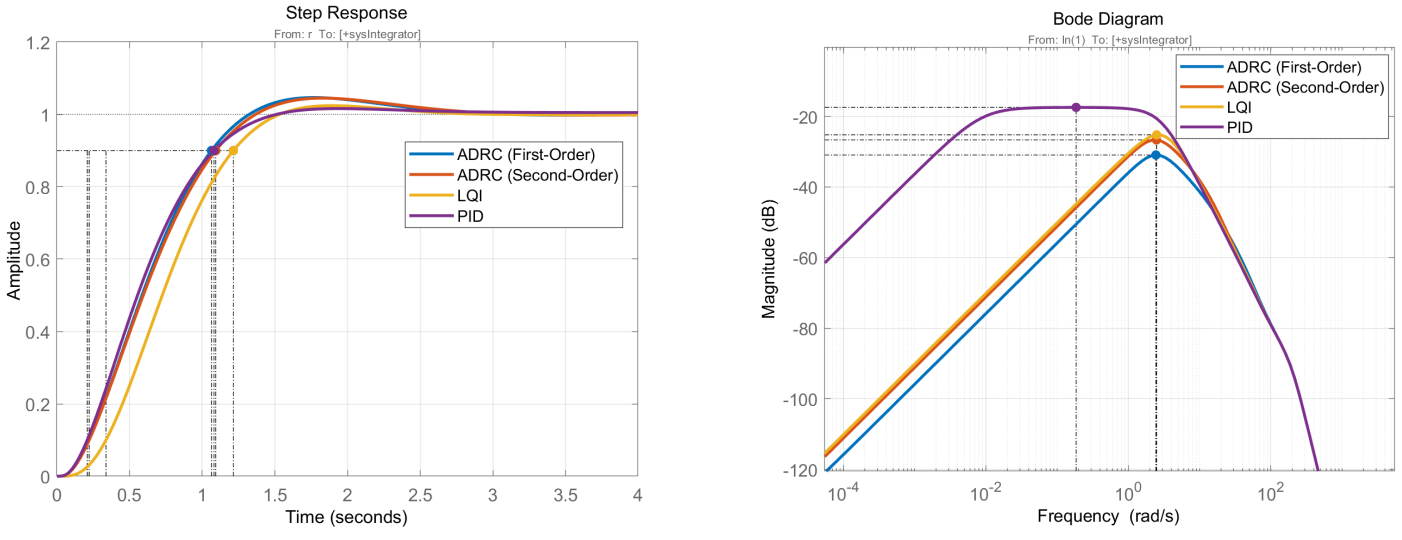
Table 2 summarizes the nominal roll-channel parameters used in the simulations.

Table 2. Roll-channel model parameters used in the simulations.

Symbol	Description	Value	Unit
L_p	Roll damping derivative	-0.8	s^{-1}
L_δ	Roll control-effectiveness derivative	16.3	s^{-2}
ω_{cas}	CAS actuator natural frequency	60	rad/s
ζ_{cas}	CAS actuator damping ratio	0.707	–
ω_{gyro}	Rate-gyro natural frequency	200	rad/s
ζ_{gyro}	Rate-gyro damping ratio	0.5	–

3.2. Nominal Closed-Loop Performance

The nominal closed-loop responses of the RESO–ADRC, LESO–ADRC, LQI, and PID controllers are compared for a step command in roll angle. Figure 2a shows the simulated roll-angle step responses, which exhibit similar rise times and small overshoot for all controllers. The controller gains used in the roll-attitude controllers are summarized in Table 3. Each ADRC scheme (first- and second-order) is represented by an equivalent PD structure with gains K_p and K_d, together with the bandwidth of the extended state observer ω_{ESO}. When ω_{ESO} is selected, the observer gains are obtained from a second-order characteristic polynomial $(s+\omega_{ESO})^2 = s^2 + 2\omega_{ESO}s + \omega_{ESO}^2$, which gives $\beta_1 = 2\omega_{ESO}$ and $\beta_2 = \omega_{ESO}^2$ for the second-order ESO, while the reduced first-order ESO uses $\beta_{RESO} = \omega_{ESO}$.



(**a**) (**b**)

Figure 2. (**a**) Nominal roll-angle step responses. (**b**) Magnitude–frequency plot of disturbance rejection for RESO–ADRC, LESO–ADRC, LQI, and PID controllers.

Table 4 summarizes the key closed-loop performance metrics in the nominal case. Both ADRC designs satisfy the phase- and gain-margin requirements with bandwidths comparable to LQI and PID. The RESO–ADRC achieves slightly faster rise time and similar overshoot compared with the LESO–ADRC, indicating that reducing the observer order does not degrade nominal performance.

Table 3. Gain sets used for the roll-rate controllers.

Controller	Gain Set
LQI	$(K_1, K_2, K_3, K_4, K_I) = (1.60, 0.47, 0.11, 4 \cdot 10^{-5}, 2.19)$
PID	$(K_p, K_i, K_d) = (0.46, 0.004, 0.23)$
2nd-order ADRC	$(K_p, K_d, \omega_{\mathrm{ESO}}) = (6.52, 3.82, 12.75)$
1st-order ADRC	$(K_p, K_d, \omega_{\mathrm{ESO}}) = (6.39, 3.67, 12.66)$

Table 4. Closed-loop performance metrics for the nominal case.

Controller	Phase Margin	Gain Margin	Overshoot	Rise Time	Bandwidth
ADRC (RESO)	67°	7.9 dB	4.6%	0.84 s	2.54 rad/s
ADRC (LESO)	71°	8.1 dB	4.5%	0.87 s	2.45 rad/s
LQI	66°	−21 dB	2.5%	0.88 s	2.48 rad/s
PID	70°	26 dB	1.63%	0.89 s	2.40 rad/s

3.3. Frequency-Domain Disturbance Rejection

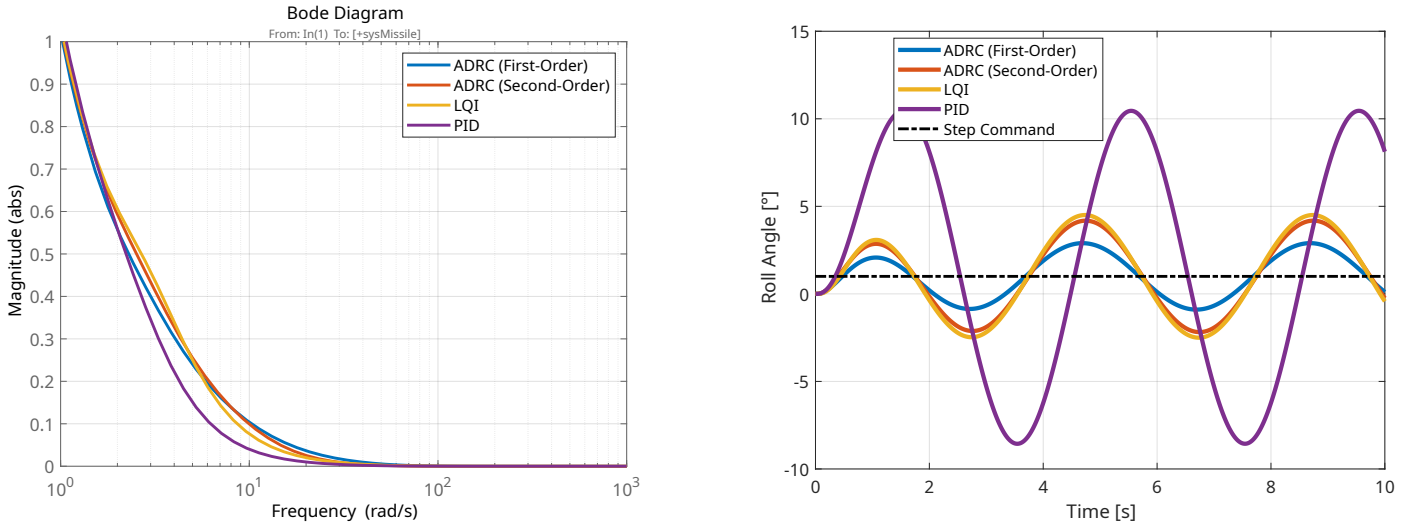
To assess input-disturbance rejection in the frequency domain, the transfer function from an additive roll-axis external disturbance to UAV dynamics [2] is derived for each controller. The magnitude Bode plots of these disturbance rejection transfer functions are shown in Figure 2b. In this figure, values below 0 dB indicate that the controllers attenuate external disturbances at the corresponding frequencies. However, the degree of attenuation varies among the controllers. The PID controller exhibits the weakest disturbance suppression over the low-frequency range of interest. The LQI and LESO–ADRC designs show similar peak disturbance rejection characteristics. The RESO–ADRC provides the best disturbance attenuation below approximately 2.5 rad/s, which corresponds to the effective bandwidth of commanded roll maneuvers. This confirms that the reduced-order observer preserves and even enhances the disturbance rejection capability of the ADRC architecture in the relevant frequency range.

3.4. Frequency-Domain Measurement Noise Rejection

The roll-rate measurement in UAVs is provided by a gyroscope, which gives a noisy measurement signal. To investigate the effect of sensor noise, the measurement noise to roll angle transfer function is analyzed, and its magnitude is plotted in Figure 3a. All four controllers behave as effective low-pass filters for gyro noise: the magnitude decreases monotonically from approximately 1 at $\omega \approx 1$ rad/s to below 0.1 for $\omega \gtrsim 10$ rad/s, which means that high-frequency measurement noise is strongly attenuated in the closed loop. The PID controller consistently yields the lowest magnitude of the noise transfer function, decreasing from about 0.4 at 3 rad/s to approximately 0.1 at 10 rad/s. The first- and second-order ADRC designs follow closely, with magnitudes typically 0.05–0.1 higher than the PID curve over the same range, while the LQI controller exhibits the largest magnitudes and therefore passes the highest amount of gyro noise. For frequencies above approximately 10 rad/s, all curves drop below 0.1 and the differences between the controllers become small. Overall, all controllers have satisfactory performance for noise rejection capability; however, PID provides the strongest noise suppression.

3.5. Time-Domain Robustness Under Disturbance and Uncertainty

To validate the frequency-domain findings, the controllers are compared in time-domain simulations under combined disturbance, noise, and parametric uncertainty. A sinusoidal external disturbance $d = 5\sin\left(\frac{\pi}{2}t\right)$ is applied to the roll axis, and zero-mean white noise with a standard deviation of $0.0167^\circ/\mathrm{s}$ is added to the gyro roll-rate measurement. The commanded roll angle is 1°, and a 20% uncertainty is introduced in the aerodynamic parameters.



(**a**) (**b**)

Figure 3. (**a**) Magnitude–frequency plot of noise rejection and (**b**) tracking performance comparison under sinusoidal external disturbance, gyro measurement noise, and aerodynamic uncertainty.

Figure 3b shows the resulting roll-angle responses. The RESO–ADRC achieves the smallest steady-state tracking error and the fastest recovery from disturbance-induced deviations, while maintaining stable behavior despite actuator dynamics, gyro dynamics, measurement noise, and parameter variations. The LESO–ADRC and LQI controllers exhibit slightly larger tracking errors and slower recovery, whereas the PID controller is more strongly affected by the external disturbance.

4. Conclusions

These results confirm that the RESO–ADRC architecture provides robust tracking and disturbance rejection capability with satisfactory noise-rejection performance for the roll channel of a small fixed-wing UAV, when compared with other autopilot architectures such as ADRC with a second-order ESO, PID, and LQI. In future work, the proposed reduced-order ADRC will be integrated into the lateral–directional control structure, including roll–yaw coupling and sideslip dynamics, and validated in hardware-in-the-loop tests to assess its robustness against actuator saturation, model uncertainty, and sensor noise.

Author Contributions: Conceptualization, F.L. and O.T.; methodology, F.L. and O.T.; software, F.L.; validation, F.L. and O.T.; formal analysis, F.L.; investigation, F.L.; resources, O.T.; data curation, F.L.; writing—original draft preparation, F.L.; writing—review and editing, F.L. and O.T.; visualization, F.L.; supervision, O.T. All authors have read and agreed to the published version of the manuscript.

Funding: This research received no external funding.

Institutional Review Board Statement: Not applicable.

Informed Consent Statement: Not applicable.

Data Availability Statement: The simulation models and data that support the findings of this study are available from the corresponding author upon reasonable request.

Acknowledgments: The authors would like to thank ROKETSAN A.S. and Middle East Technical University for their support.

Conflicts of Interest: This work was carried out at Middle East Technical University as part of Furkan Leblebici's M.S. thesis work. During this period, Furkan Leblebici was employed by ROKETSAN A.S. The authors declare that the research was conducted in the absence of any commercial or financial relationships that could be construed as a potential conflict of interest.

Abbreviations

The following abbreviations are used in this manuscript:

ADRC	Active Disturbance Rejection Control
LESO	Linear Extended State Observer
RESO	Reduced-Order Extended State Observer
LQI	Linear Quadratic Integral
PID	Proportional–Integral–Derivative
UAV	Unmanned Aerial Vehicle

References

1. Talole, S.E.; Kolhe, V.R.; Bhattacharyya, S.P. Robust Roll Autopilot Design for Tactical Missiles. *J. Guid. Control Dyn.* **2011**, *34*, 1872–1884. [CrossRef]
2. Gezer, R.B.; Kutay, A.T. Robust Model Following Control Design for Missile Roll Autopilot. In Proceedings of the 2014 UKACC International Conference on Control (CONTROL), Loughborough, UK, 9–11 July 2014; pp. 7–12. [CrossRef]
3. Ali, K.M. Design of a Roll Autopilot for a Skid-to-Turn Guided Missile. *ASAT J.* **2019**. Available online: https://iopscience.iop.org/article/10.1088/1757-899X/610/1/012017/pdf (accessed on 1 November 2025).
4. Xu, X.; Cui, X.; Yu, W.; Luo, P.; Gao, M. Design of Missile Roll Autopilot Based on Linear Extended State Observer. In Proceedings of the 2022 34th Chinese Control and Decision Conference (CCDC), Hefei, China, 15–17 August 2022; pp. 418–421.
5. Marwan, H.; Humaidi, A.J.; Al-Khazraji, H. Active Disturbance Rejection Control for Unmanned Aerial Vehicle. *Int. J. Robot. Control Syst.* **2025**, *5*, 1278–1296. [CrossRef]
6. Han, J. From PID to Active Disturbance Rejection Control. *IEEE Trans. Ind. Electron.* **2009**, *56*, 900–906. [CrossRef]
7. Gao, Z. Active Disturbance Rejection Control: A Paradigm Shift in Feedback Control. In Proceedings of the 2006 American Control Conference, Minneapolis, MN, USA, 14–16 June 2006; pp. 2399–2405.
8. Sun, Z.; Wu, L.; Guo, Z.; Zhang, H. Research on Roll Attitude Control of UAV Based on Active Disturbance Rejection Control. *IOP Conf. Ser. Earth Environ. Sci.* **2020**, *428*, 012083. [CrossRef]
9. Zhang, Y.; Wang, S.; Dong, C.; Zhou, H. A Novel Control Scheme for Quadrotor UAV Based upon Active Disturbance Rejection Control and Model-Free Adaptive Control. *ISA Trans.* **2019**, *79*, 65–77.
10. Qi, D.; Zhang, R.; Chen, L. Dynamic Model and Active Disturbance Rejection Control of a Novel Water–Air Unmanned Vehicle. *J. Vibroeng.* **2016**, *18*, 1309–1321. [CrossRef]
11. Ding, X.; Hu, Y.; Jia, R.; Guo, J. A Novel Disturbance Rejection Control of Roll Channel for Small Air-to-Surface Missiles. *Appl. Sci.* **2023**, *13*, 389. [CrossRef]
12. Godbole, A.A.; Talole, S.E.; Bhattacharyya, S.P. Extended State Observer-Based Robust Pitch Autopilot Design for Tactical Missiles. *Proc. Inst. Mech. Eng. G J. Aerosp. Eng.* **2012**, *226*, 1125–1141. [CrossRef]
13. Wang, X.; Kong, W.; Zhang, D.; Shen, L. Active Disturbance Rejection Controller for Small Fixed-Wing UAVs with Model Uncertainty. In Proceedings of the 2015 IEEE International Conference on Information and Automation (ICIA), Lijiang, China, 8–10 August 2015; pp. 2299–2304. [CrossRef]
14. Zhong, S.; Huang, Y. Quantitative Analysis on the Phase Margin of ADRC. *Control Theory Technol.* **2023**, *21*, 4–15. [CrossRef]

15. The MathWorks Inc. *MATLAB*, Version R2023a; The MathWorks Inc.: Natick, MA, USA, 2023.
16. Gao, Z. Scaling and Bandwidth-Parameterization Based Controller Tuning. In Proceedings of the 2003 American Control Conference (ACC), Denver, CO, USA, 4–6 June 2003; pp. 4989–4996. [CrossRef]

Disclaimer/Publisher's Note: The statements, opinions and data contained in all publications are solely those of the individual author(s) and contributor(s) and not of MDPI and/or the editor(s). MDPI and/or the editor(s) disclaim responsibility for any injury to people or property resulting from any ideas, methods, instructions or products referred to in the content.